

Supplementary Materials

The Impact of Polymerization Atmosphere on the Microstructure and Photocatalytic Properties of Fe-Doped g-C₃N₄ Nanosheets

Xiaoyu Peng, Xiufang Chen *, Rui Pang, Lanlan Cheng, Fengtao Chen and Wangyang Lu

National & Local Joint Engineering Research Center for Textile Fiber Materials and Processing Technology, College of Material Science and Engineering, Zhejiang Sci-Tech University, Hangzhou 310018, China; xiaoyu_peng@163.com (X.P.); 19857115160@163.com (R.P.); cll73739703@163.com (L.C.); cft0923@163.com (F.C.); luwy@zstu.edu.cn (W.L.)

* Correspondence: chenxf@zstu.edu.cn

1. Experimental section

1.1. Materials

Urea (CH₄N₂O) was purchased from Tianjin Wing Tai Chemical Co., Ltd. Carbamazepine (CBZ, C₁₅H₁₂N₂O), ferric nitrate nonahydrate (Fe(NO₃)₃·9H₂O), sodium chloride (NaCl), sodium nitrate (NaNO₃), sodium sulphate (Na₂SO₄), sodium carbonate (NaCO₃), sodium chloroacetate (ClCH₂COONa), sodium hydroxide (NaOH), methanol (CH₄O), 5,5-dimethyl-1-pyrroline N-oxide (DMPO, C₆H₁₁NO), 2,2,6,6-Tetramethylpiperidine (TEMP, C₉H₂₀N₂), p-Benzoquinone (p-BQ, C₆H₄O₂), L-Histidine (L-His, C₆H₉N₃O₂), and tert-Butanol (TBA, C₄H₁₀O) were purchased from Shanghai Aladdin Biochemical Technology Co., Ltd. Ethanol (EA, C₂H₆O) was purchased from Hangzhou Gaojing Fine Chemical Co., Ltd. Concentrated sulfuric acid (H₂SO₄) was purchased from Hangzhou Shuanglin Chemical Reagent Co., Ltd.

1.2. Synthesis of Fe-doped g-C₃N₄ catalyst

Briefly, 10 g of urea and a certain amount of ferric nitrate were dissolved in 25 mL of deionized water, and then stirred vigorously at 80 °C overnight to remove water completely. The mixture was placed in a covered ceramic crucible and heated in a muffle furnace at 550 °C for 2 h. The obtained product was named FeN_x-CNO. The mixture was calcined in nitrogen gas at 550 °C for 2 h, and the obtained product was named FeN_x-CNN.

1.3. Characterization

The chemical structures of synthesized g-C₃N₄-based photocatalysts were characterized by X-ray diffractometer (XRD, D8 Discover, Germany), Fourier transform infrared spectrometer (FT-IR, Nicolet 5700, Germany), and X-ray photoelectron spectrometer (XPS, Thermo Scientific K-Alpha, America). The morphology of the catalysts was analyzed by field emission scanning electron microscope (SEM-EDS, Gemini-500, Germany) and transmission electron microscope (TEM, JEM-2100, Japan). The Brunauer–Emmett–Teller (BET) surface area and pore volume of the prepared catalysts were calculated from N₂ adsorption isotherms at liquid N₂ temperature using a surface area and porosity analyzer (BET, Micromeritics APSP 2460, America). The optical absorption and bandgap (E_g) energy of the as-prepared catalytic samples was illustrated by UV–Vis diffuse reflectance spectra (DRS, Lambda 950 PerkinElmer). The photoluminescence property was characterized by

photoluminescence (PL) spectrophotometer (F-4600, Hitachi, Japan). An electron paramagnetic resonance spectrometer (EPR, A300, Bruker, Germany) was employed to determine various reactive radical species ($\text{SO}_4^{\bullet-}$, $\bullet\text{OH}$, $\text{O}_2^{\bullet-}$, and $^1\text{O}_2$) captured by DMPO or TEMP in the photocatalytic system. UPLC/HDMS in positive ion mode was used to detect the intermediates generated during the degradation of CBZ by $\text{FeN}_x\text{-CNO}$ -activated PMS.

1.4 Photocatalytic tests

The photocatalytic performance of the prepared catalysts was evaluated by photodegradation of CBZ in a 40 mL clear glass reaction vial at room temperature. Specifically, a simulated UV–vis light source was generated in a Q-Sun Xe1 (USA) test chamber. Prior to the light reaction, 2 mg of catalyst was dispersed in 20 ml of CBZ (2.5 mM) solution and sonicated for 5 min, and then the reaction was carried out for 20 min using PMS (0.2 mM) as the oxidant. The concentration of CBZ solution was detected by ultrahigh-performance liquid chromatography (HPLC, Waters, America). An acetonitrile and water eluent with a volume ratio of 40:60 with the flow rate at 0.30 mL min^{-1} was employed as the mobile phase. The photodegradation efficiency was assessed by C/C_0 , whereas C_0 and C represent the original CBZ concentration and that remaining in the reaction CBZ mixture after some time, respectively. In the reusability tests, the catalyst was separated by filtration, fully washed with water, and dried after each cycle, and then used for the next run. The mineralization rate was measured by total organic carbon analyzer (TOC-LCPH, Shimadzu, Japan). In the acidic or alkaline systems, the pH was adjusted by $0.1\text{ mol L}^{-1}\text{ H}_2\text{SO}_4$ or NaOH addition prior to irradiation.

Figures

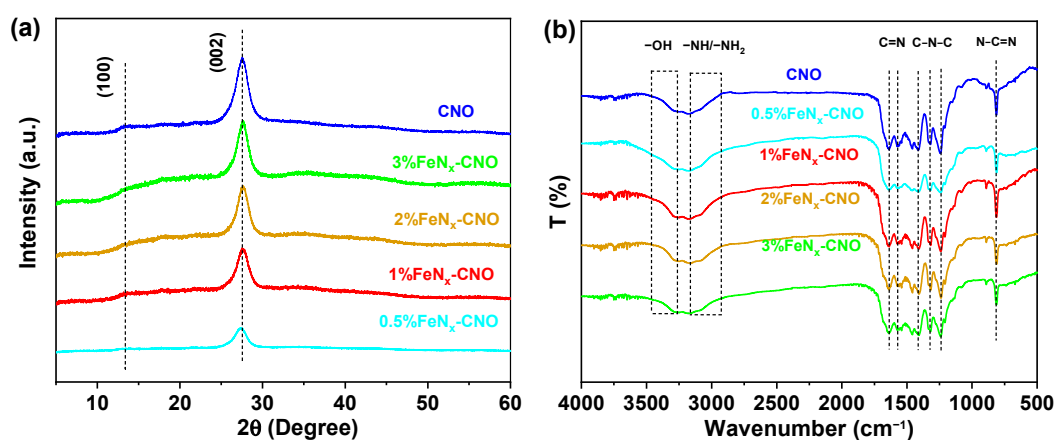


Figure S1. (a) XRD patterns and (b) FT-IR spectra of $n\%\text{FeN}_x\text{-CN}$.

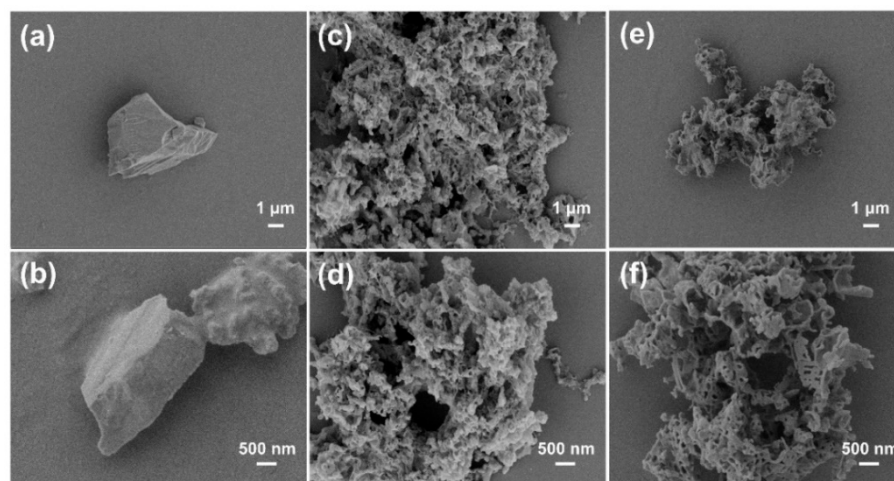


Figure S2. SEM images of (a, b) bulk 1%FeN_x-CN, (c, d) 1%FeN_x-CNO, and (e, f) 1%FeN_x-CCN at different magnifications.

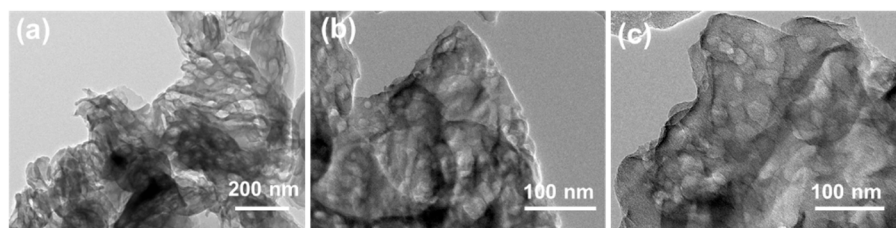


Figure S3. TEM images of (a-c) g-C₃N₄.

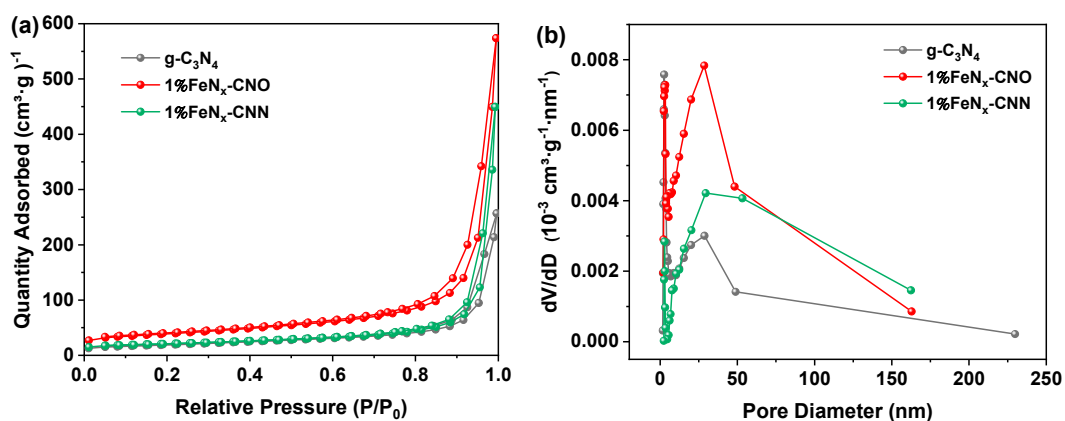


Figure S4. (a) Nitrogen adsorption–desorption isotherms and (b) pore size distributions of g-C₃N₄, 1%FeN_x-CNO, and 1%FeN_x-CNN.

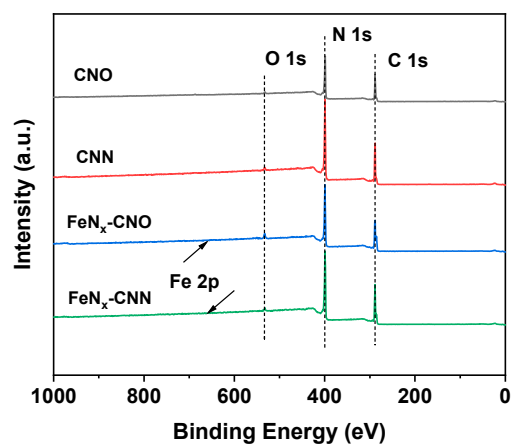


Figure S5. XPS full Spectrum of CNO, CNN, 1%FeN_x-CNO, and 1%FeN_x-CNN.

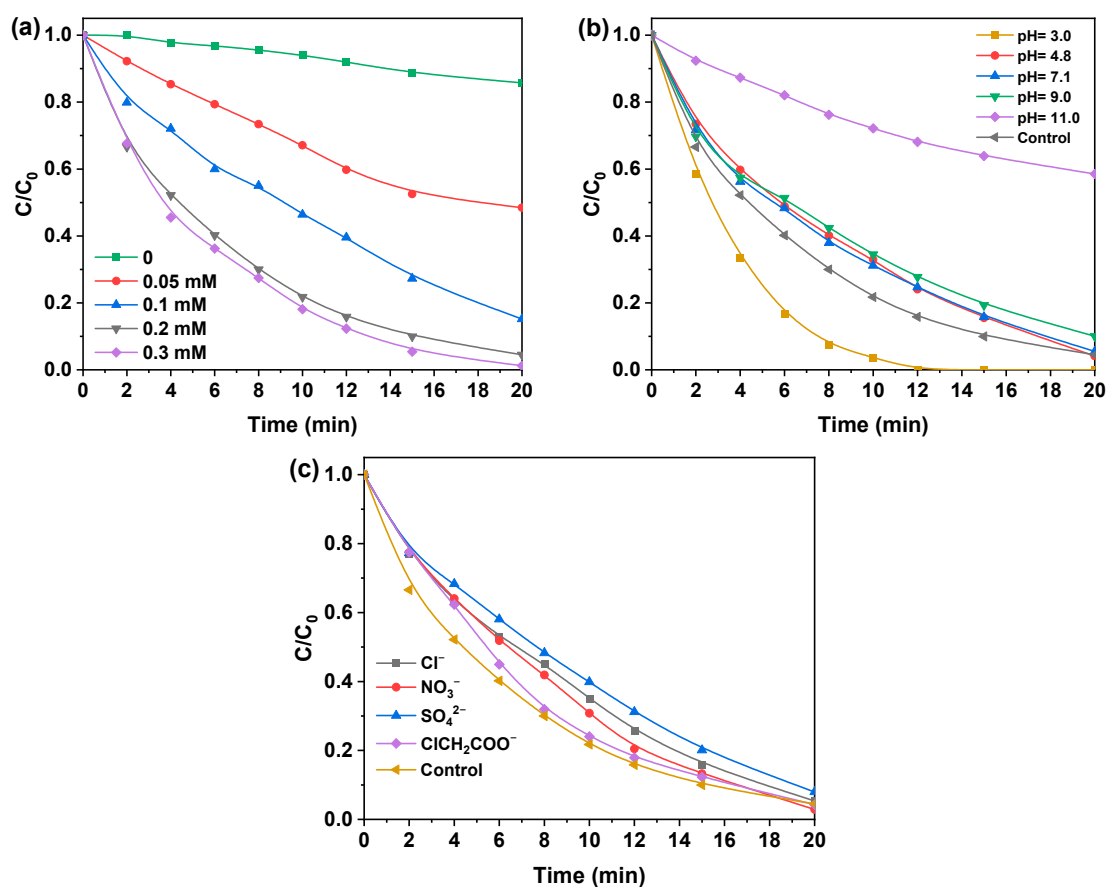


Figure S6. The photocatalytic activity of 1%FeN_x-CNO under (a) different concentrations of PMS, (b) different pH conditions, and (c) different inorganic salt ions.

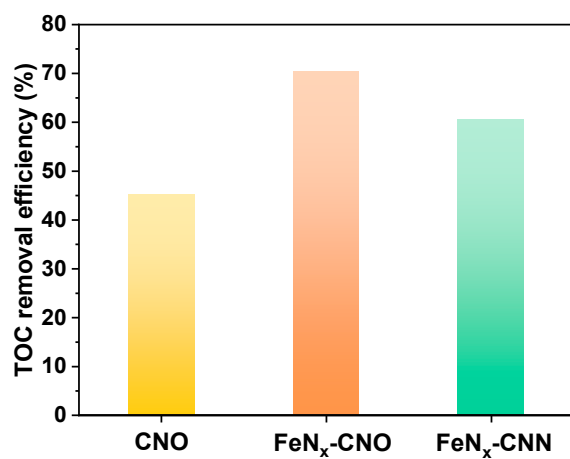


Figure S7. TOC removal rate after 120 min photocatalytic reaction of CNO/PMS, FeN_x-CNO/PMS, and FeN_x-CNN/PMS systems.

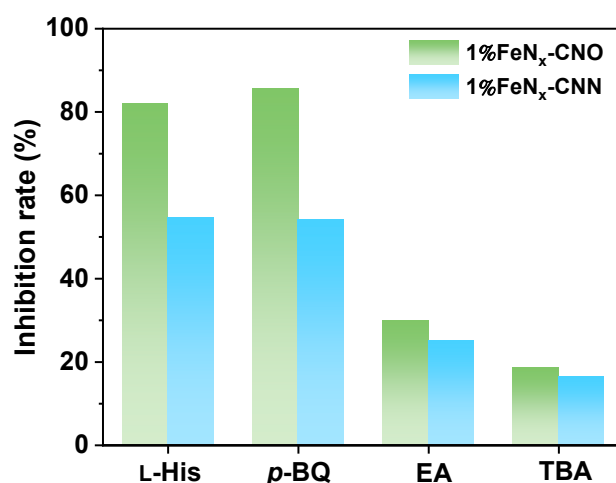


Figure S8. Comparison of inhibition rates of (a) FeN_x-CNO and (b) FeN_x-CNN for photocatalytic degradation of CBZ by different trapping agents.

Tables

Table S1. BET surface areas, pore volumes, and pore average diameter of various samples.

Samples	S _{BET} (m ² g ⁻¹)	V _p (cm ³ g ⁻¹)	D _p (nm)
g-C ₃ N ₄	66.3	0.393	26.8
1%FeN _x -CNO	136.2	0.874	31.7
1%FeN _x -CNN	74.2	0.688	46.5

Table S2. Proportion of different chemical bonds about C atoms in different samples.

	CNO	1%FeN _x -CNO	CNN	1%FeN _x -CNN
C-C	12.8	28.8	11.5	18.3
C-NH _x	3.1	3.7	2.6	2.3
C-N=C	84.1	67.5	85.9	79.4

Table S3. Proportion of different chemical bonds about O atoms in different samples.

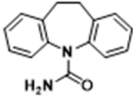
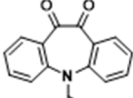
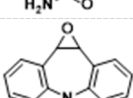
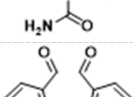
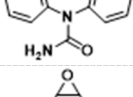
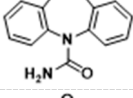
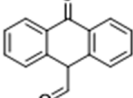
	CNO	1%FeN _x -CNO	CNN	1%FeN _x -CNN
O _v	31.1	48.3	41.4	40.7
O _s	68.9	51.7	58.6	59.3

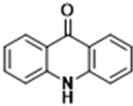
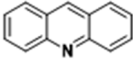
Table S4. Comparison of photocatalytic performance of various catalysts for CBZ degradation in the presence of PMS.

Entry	Catalyst	Conditions	Light source	Reaction time	Conversion	Ref.
1	g-C ₃ N ₄ (KPS)	[Catalyst] = 0.1 g/L, [CBZ] = 2.5×10 ⁻⁵ M, [PMS] = 4×10 ⁻⁴ M	xenon lamp 300 W	20 min	95.4%	[61]
2	VL/Bi ₂ WO ₆	[Catalyst] = 1 g/L, [CBZ] = 4.3×10 ⁻⁵ M, [PMS] = 2.5×10 ⁻³ M	xenon lamp 300 W	120 min	85%	[62]
3	g-C ₃ N ₄ -IMA-FePcCl ₁₆	[Catalyst] = 0.1 g/L, [CBZ] = 2.5×10 ⁻⁵ M, [PMS] = 3×10 ⁻⁴ M	xenon lamp 300 W	25 min	95%	[63]

4	10% Ag ₃ PO ₄ @TPC N ₁₂	[Catalyst] = 0.3 g/L, [CBZ] = 8.5×10 ⁻⁶ M, [PMS] = 4.5×10 ⁻⁴ M	xenon lamp 300 W (λ > 420 nm)	45 min	100%	[64]
5	ABF-5 (AgBr/Bi- OBr/Fe ₃ O ₄)	[Catalyst] = 0.3 g/L, [CBZ] = 4.3×10 ⁻⁵ M, [PMS] = 6×10 ⁻⁴ M	xenon lamp 500 W (λ > 400 nm)	30 min	96%	[65]
6	CoFe ₂ O ₄ /rGO	[Catalyst] = 0.2 g/L, [CBZ] = 2.15×10 ⁻⁴ M, [PMS] = 9×10 ⁻⁴ M	LED	30 min	93.2%	[66]
7	g-C ₃ N ₄ -INA- FePcCl ₁₆	[Catalyst] = 0.1 g/L, [CBZ] = 2.5×10 ⁻⁵ M, [PMS] = 1.8×10 ⁻⁴ M	xenon lamp 300 W	40 min	94%	[67]
8	H-CTF-Na	[Catalyst] = 0.4 g/L, [CBZ] = 2.2×10 ⁻⁵ M, [PMS] = 1.3×10 ⁻³ M	xenon lamp 300 W (λ > 400 nm)	100 min	96.8%	[68]
9	EPT _{0.05} &PS	[Catalyst] = 1 g/L, [CBZ] = 2.15×10 ⁻⁵ M, [PMS] = 1×10 ⁻³ M	xenon lamp 300 W (λ > 420 nm)	30 min	97.1%	[69]
10	1%FeN _x -CNO	[Catalyst] = 0.1 g/L, [CBZ] = 2.5×10 ⁻⁵ M, [PMS] = 2×10 ⁻⁴ M	xenon lamp 300 W	20 min	96%	This work

Table S5. The intermediate products formed during the degradation of CBZ by FeN_x-CNO/PMS/Light system were detected by UPLC/HDMS in positive ion mode.

Molecular formula	Structural formula	Retention time(min)	Theoretical Mass(m/z)	Measured Mass (m/z)	mDa
CBZ (C ₁₅ H ₁₂ N ₂ O)		4.81	237.1028	237.1037	+0.9
A (C ₁₅ H ₁₀ N ₂ O ₃)		3.66	267.0770	267.0767	-0.3
B (C ₁₅ H ₁₂ N ₂ O ₂)		4.08	253.0977	253.0971	-0.6
C (C ₁₅ H ₁₂ N ₂ O ₃)		3.90	269.0926	269.0926	0
D (C ₁₅ H ₁₂ N ₂ O ₂)		3.86	251.0816	251.0827	+1.1
E (C ₁₄ H ₉ NO ₂)		1.12	224.0712	224.0710	-0.2
F (C ₁₄ H ₉ NO)		3.88	208.0762	208.0764	+0.2

G (C ₁₃ H ₉ NO)		4.47	196.0762	196.0755	-0.7
H (C ₁₃ H ₉ N)		5.93	180.0815	180.0822	+0.7

References

- Mei, X.; Chen, S.; Wang, G.; Chen, W.; Lu, W.; Zhang, B.; Fang, Y.; Qi, C. Metal-free Carboxyl Modified g-C₃N₄ for Enhancing Photocatalytic Degradation Activity of Organic Pollutants Through Peroxymonosulfate Activation in Wastewater under Solar Radiation. *J. Solid State Chem.* **2022**, *310*, 123053.
- Qi, Y.; Zhou, X.; Li, Z.; Yin, R.; Qin, J.; Li, H.; Guo, W.; Li, A.; Qiu, R. Photo-Induced Holes Initiating Peroxymonosulfate Oxidation for Carbamazepine Degradation via Singlet Oxygen. *Catalysts* **2022**, *12*, 1327.
- Dong, L.; Xu, T.; Chen, W.; Lu, W. Synergistic Multiple Active Species for the Photocatalytic Degradation of Contaminants by Imidazole-Modified g-C₃N₄ Coordination with Iron Phthalocyanine in the Presence of Peroxymonosulfate. *Chem. Eng. J.* **2019**, *357*, 198–208.
- Li, J.; Huang, W.; Yang, L.; Gou, G.; Zhou, C.; Li, L.; Li, N.; Liu, C.; Lai, B. Novel Ag₃PO₄ Modified Tubular Carbon Nitride with Visible-light-driven Peroxymonosulfate Activation: A Wide pH Tolerance and Reaction Mechanism. *Chem. Eng. J.* **2022**, *432*, 133588.
- Tao, Y.; Fan, G.; Li, X.; Cao, X.; Du, B.; Li, H.; Luo, J.; Hong, Z.; Xu, Q. Recyclable Magnetic AgBr/BiOBr/Fe₃O₄ Photocatalytic Activation Peroxymonosulfate for Carbamazepine Degradation: Synergistic Effect and Mechanism. *Ser. Purif. Technol.* **2024**, *330*, 125392.
- Zhang, Y.; Cheng, Y.; Qi, H. Synergistic Degradation of Organic Pollutants on CoFe₂O₄/rGO Nanocomposites by Peroxymonosulfate Activation under LED Irradiation. *Appl. Surf. Sci.* **2022**, *579*, 152151.
- Wu, F.; Huang, H.; Xu, T.; Lu, W.; Li, N.; Chen, W. Visible-Light-Assisted Peroxymonosulfate Activation and Mechanism for the Degradation of Pharmaceuticals over Pyridyl-Functionalized Graphitic Carbon Nitride Coordinated with Iron Phthalocyanine. *Appl. Catal. B Environ.* **2017**, *218*, 230–239.
- Zeng, T.; Li, S.; Shen, Y.; Zhang, H.; Feng, H.; Zhang, X.; Li, L.; Cai, Z.; Song, S. Sodium Doping and 3D Honeycomb Nanoarchitecture: Key Features of Covalent Triazine-based Frameworks (CTF) Organocatalyst for Enhanced Solar-driven Advanced Oxidation Processes. *Appl. Catal. B Environ.* **2019**, *257*, 117915.
- Yang, L.; Jia, Y.; Peng, Y.; Zhou, P.; Yu, D.; Zhao, C.; He, J.; Zhan, C.; Lai, B. Visible-light Induced Activation of Persulfate by Self-assembled EHPDI/TiO₂ Photocatalyst toward Efficient Degradation of Carbamazepine. *Sci. Total Environ.* **2021**, *783*, 146996.